

Systematic control of surface Dirac fermion density on topological insulator Bi_2Te_3

Y. Xia,¹ D. Qian,^{1,2} D. Hsieh,¹ R. Shankar,¹ H. Lin,³ A. Bansil,³ A. V. Fedorov,⁴ D. Grauer,⁵ Y. S. Hor,⁵ R. J. Cava,⁵ and M. Z. Hasan^{1,6,7}

¹Joseph Henry Laboratories of Physics, Department of Physics,
Princeton University, Princeton, NJ 08544, USA

²Department of Physics, Shanghai Jiao Tong University, Shanghai 200030, China

³Department of Physics, Northeastern University, Boston, MA

⁴Advanced Light Source, Lawrence Berkeley National Laboratory,
University of California, Berkeley, CA 94305, USA

⁵Department of Chemistry, Princeton University, Princeton, NJ 08544, USA

⁶Princeton Center for Complex Materials,
Princeton University, Princeton, NJ 08544, USA

⁷Princeton Institute for the Science and Technology of Materials,
Princeton University, Princeton, NJ 08544, USA

(Dated: February 22, 2024)

Abstract

Three dimensional (3D) topological insulators are quantum materials with a spin-orbit induced bulk insulating gap that exhibit quantum Hall-like phenomena in the absence of applied magnetic fields. They feature surface states that are topologically protected against scattering by time-reversal symmetry. The proposed applications of topological insulators in device geometries rely on the ability to tune the chemical potential on their surfaces in the vicinity of the Dirac node. Here, we demonstrate a suite of surface control methods based on a combination of photo-doping and molecular-doping to systematically tune the Dirac fermion density on the topological (111) surface of Bi_2Te_3 . Their efficacy is demonstrated via direct electronic structure topology measurements using high resolution angle-resolved photoemission spectroscopy. These results open up new opportunities for probing topological behavior of Dirac electrons in Bi_2Te_3 . At least one of the methods demonstrated here can be successfully applied to other topological insulators such as the bulk-insulating $\text{Bi}_{1-x}\text{Sb}_x$, Sb_2Te_3 and Bi_2Se_3 which will be shown elsewhere. More importantly, our methods of topological surface state manipulation demonstrated here are highly suitable for future spectroscopic studies of topological phenomena which will complement the transport results gained from the traditional electrical gating techniques.

Recently, there has been a surge of research interest in the newly discovered class of 3D time reversal invariant topological insulators [1, 2, 3, 4, 5, 6] both from the fundamental physics and potential application viewpoints. Such systems have been proposed to exhibit many exotic quantum phenomena [7, 8, 9] that can be realized in condensed-matter tabletop settings. Three dimensional topological insulator phases with gapless topological edge states have been observed in Bi_4Sb_x [10, 12], Bi_2Se_3 [11] and Bi_2Te_3 [13, 14, 15]. Topological order (the physically observable quantity that uniquely characterizes the new state, and in some sense comes closest to an "order parameter" of the state in the absence of the spontaneously broken symmetry unlike that in a superconductor) in a topological insulator cannot be determined without spin-texture or Berry's phase imaging measurements. Using spin-resolved methods, Hsieh et al. measured the Berry's phase texture of the Bi_4Sb_x and Bi_2Te_3 classes of material [12, 14], confirming the Fu-Kane-Mele type \mathbb{Z}_2 topological order [4, 5, 6] in these materials. In the momentum space, the pairs of time-reversal invariant edge states can be described as massless Dirac fermions inside the bulk band-gap. A strong topological insulator (STI) is the one characterized by having an odd number pair of such states, which are topologically protected against backscattering. The STI phase is a topologically distinct novel phase of matter and cannot be adiabatically reduced to the quantum spin Hall phase proposed in the strongly spin-orbit coupled two dimensional electron gases [16]. It is the surface dynamics and control of topological Dirac fermions in the Bi_2Te_3 class that we focus in this paper.

While the density of state at the Fermi level ($\text{DOS}(E_F)$) in a conventional quantum Hall system (QHE in 2DEG) can be tuned via an external magnetic field, this method cannot be applied to the STIs for a magnetic field breaks time reversal symmetry and the topological protection is thus lost. Furthermore, chemical techniques such as the bulk doping to reach the Dirac point are undesirable as they introduce extra carriers which either turn the bulk into a semiconductor or an alloy or increase the residual conductivity beyond the surface conduction limit. None of these conditions are desirable for a functional topological insulator. Here, we demonstrate a suite of surface doping methods which can tune the carrier density on the surfaces of the topological insulator system Bi_2Te_3 in a time-reversal invariant way. Using angle-resolved photoemission spectroscopy, we demonstrate the capability of electronic structure engineering of the Bi_2Te_3 surface with alkali atom (potassium, K) deposition, molecular adsorption and photo-doping without breaking the time reversal or

the Z_2 invariance. We show that the chemical potential can be systematically tuned to shift the surface Dirac point downwards in energy. Moreover, we report that the effect of NO_2 molecular adsorption can be further manipulated by photon-assisted stimulation, thereby controlling the surface carrier density in the opposite directions. These methods of tuning carrier densities on the surface of a topological insulator open up new research avenues for spintronic and quantum computing applications where the control of the density of Dirac fermions on the surfaces is critical to observe many spin-orbit or spintronic quantum effects. More importantly, our methods of topological surface state manipulation, highly suitable for spectroscopic studies, demonstrated here will complement the traditional electrical gating techniques.

Single crystal of Bi_2Te_3 was grown by melting stoichiometric mixtures of high purity elemental Bi (99.999%) and Te (99.999%) in a vacuum sealed 4 mm inner diameter quartz tube at 800 °C. The sample was then cooled over a period of two days to 550 °C, and then annealed at that temperature for 5 days. A single crystal with lowest residual conductivity characterized via transport methods was obtained. Single crystals could be easily cleaved along the basal plane. The crystal was confirmed to be single phase and identified as having the rhombohedral crystal structure by X-ray powder diffraction using a Bruker D8 diffractometer with Cu K α radiation and a graphite diffracted beam monochromator.

High-resolution ARPES measurements were then performed using 30 to 55 eV photons at Beam line 12.0.1 of the Advanced Light Source in Lawrence Berkeley National Laboratory. The energy and momentum resolution were typically 15 meV and 1.5% of the surface Brillouin Zone (BZ) respectively using a Scienta analyzer. The in-plane crystal orientation was determined by Laue x-ray diffraction prior to inserting into the ultra-high vacuum measurement chamber. The samples were cleaved in situ at 10K under pressures of less than 2×10^{-11} torr, resulting in shiny flat surfaces. NO_2 molecular doping of the Bi_2Te_3 surface was achieved via controlled exposures to NO_2 gas (Matheson, 99.5%), after the surface was allowed to relax for 1 hour after cleavage [14]. The adsorption effects were studied under static flow mode: exposing the sample to the gas for a certain time then taking data after the chamber was pumped down to the base pressure. The sample temperature was maintained at 10K during exposure to NO_2 . For K deposition, a heated K evaporation source was used operating at 5.5 Å. We also present band calculations for the Bi_2Te_3 (111) surface with parameters optimized based on experimental data, which were performed with the LAPW method

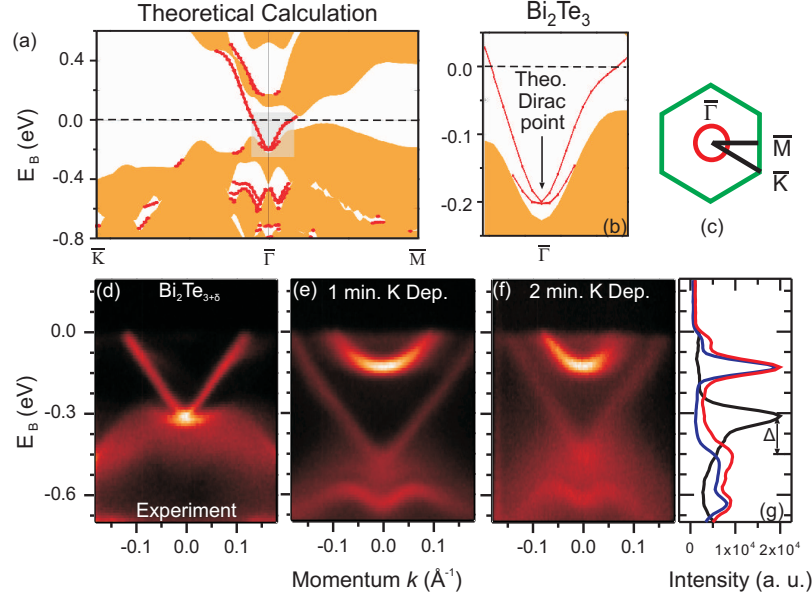


FIG. 1: Electron doping via potassium (K) deposition on Bi_2Te_3 [111] topological surface : (a)–(b) (111) Surface band (red lines) calculation with spin-orbit coupling shows a pair of non-degenerate Dirac bands crossing the E_F . The bulk band projection is denoted by the shaded region in orange. The resulting (c) Fermi surface is a single non-degenerate ring centered at the zone center. (d) ARPES data on $\text{Bi}_2\text{Te}_{3+\delta}$ shows a slight rise of the chemical potential relative to the stoichiometric compound Bi_2Te_3 [14]. The surface band structure after depositing potassium (K) for (e) one minute and (f) two minutes show additional electron-doping of the surface states. The (g) energy distribution curves at show that relative to the pristine sample (black), the chemical potential is shifted by 140 meV after one minute of (red) of K deposition. Only a small additional shift of the E_F position is observed upon an additional minute of K deposition (blue).

in slab geometry using the WIEN2K package [17]. The calculated band-structure was found to be qualitatively similar to previous report calculated using different methods [18]. GGA of Perdew, Burke, and Ernzerhof [19] was used to describe the exchange-correlation potential with SOC included as a second variational step. The surface was simulated by placing a slab of six quintuple layers in vacuum. A grid of $35 \times 35 \times 1$ points were used in the calculations, equivalent to 120 k-points in the irreducible BZ and 2450 k-points in the first BZ.

Calculated band structure along the $\text{K} - \text{M}$ direction shows that spin-orbit coupling induces a single metallic surface band near the zone center (Fig. 4 (a)–(b)). The resulting surface Fermi surface is a single non-degenerate ring centered at Γ . Although the experi-

experimental results are in qualitative agreement with calculations and the chemical potential lies in the gap only intersecting the surface states (Fig.1), the observed differences could result from the fact that all Bi_2Te_3 samples have a relaxed cleaved surface [13, 14]. Because of details of the surface relaxation (thus band bending) of Bi_2Te_3 has no simple correlation with the bulk carrier concentration (insulating or not) of our samples it is not possible to find a unique fingerprint of the bulk insulating state by just studying the surface Fermi surface shape. We have experimentally determined that in the presence of relaxation, slightly excess Te atoms added in the bulk can electron dope the surface (Figure 1(d)). These effects taken together may account for some of the differences between calculated band structure and the experimental data.

In Figure 4(e)) we present ARPES data taken at 30 eV after potassium (K) is deposited onto the sample for approximately one minute. The material becomes strongly electron doped, with the bottom of the "V" (Dirac band) band rigidly shifted by approximately 140 meV. The Fermi velocity of the Dirac band is unchanged with doping. In addition, we observe an inner resonant-state (due to surface band bending) feature that appears to be the bottom of a pair of spin-split parabolic bands shifted from each other in k -space. These bands are reminiscent of those observed in the SS of Au(111) and Sb(111) at Γ . Assuming that each K atom donates one electron, Luttinger count theorem suggests that the change of the electron pocket size corresponds to 7% of a K monolayer deposited onto the sample surface. Additional K doping (Fig. 4(f)) has little effect on moving the chemical potential. The signal from the Dirac point however attenuates due to the increasing escape depth of the photoelectrons (Fig. 4(g)). Nevertheless, no gap is observed as a result of deposition, confirming that time-reversal symmetry is preserved suggesting the non-magnetic character of the valence state of K sticking onto the surface.

We then study the effect of NO_2 doping on the Bi_2Te_3 (111) surface states which has been shown to be effective in graphene [20, 21]. To check the adsorption or sticking behavior of the molecular dopants, Figure 5(a)–(d) we collect valence data with a wide binding energy range above 15 eV prior and post exposure of the NO_2 gas. On the clean undoped samples (Fig. 5(a)–(b)), dispersive Bi_2Te_3 valence bands are clearly observed at binding energies from 0 to 5 eV, with some additional weak features at binding energies of 9–11 eV characterizing the Bi_2Te_3 matrix. Upon exposure to NO_2 , three additional intense features appear at binding energies of 4.4 eV, 7.5 eV and 13 eV (Fig. 5(c)–(d)). These new features are non-dispersive

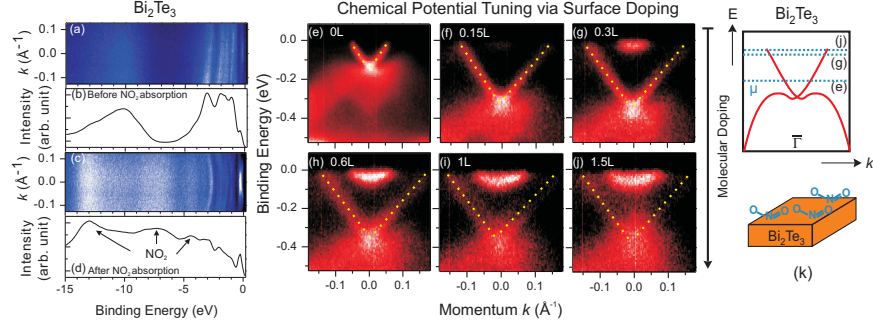


FIG. 2: Manipulation of Bi_2Te_3 [111] topological surface via molecular adsorption: (a) Angle-resolved valence band spectra (a) prior to and (c) post exposure to 1.5 Langmuirs of NO_2 . Panels (b) and (d) show the angle integrated spectra for (a) and (c), respectively. Prior to the NO_2 adsorption, the valence band features are sharp and dispersive with momentum. After exposure to NO_2 gas, three non-dispersive features appear at binding energies of 4.4 eV, 7.5 eV and 13 eV. High resolution surface band dispersion data near the Γ point suggest (e) two non-degenerate surface bands intersecting at 130 meV below E_F , forming a Dirac point. (f)–(j), with NO_2 adsorption, the chemical potential is systematically raised, thereby introducing additional electrons into the Bi_2Te_3 surface bands. The Dirac point moves away from E_F with increasing amounts of NO_2 exposure. At 1 Langmuir dosage value, the lowest surface conduction band gains electron occupation, and the Dirac point reaches 350 meV below E_F .

and independent of the choice of incident photon energy, which suggest that they are due to the adsorbed distributed molecules on the sample surface. Core level signals at similar binding energies are known to appear upon depositing NO_2 on carbon-based materials [21]. These results confirm the sticking or adsorption of NO_2 on Bi_2Te_3 (111) surface.

The surface band dispersions near Γ with varying NO_2 dosages are shown in Fig. 5 (e)–(j). After equal intervals of data collection time, one finds two significant changes in the photoemission spectra. Firstly, due to an increasing surface roughness, the measured spectra after NO_2 exposure are not as sharp as that from a clean surface. The total emission intensity is reduced, as the photoelectron escape depth is increased. Secondly, after NO_2 adsorption, the electron pocket around Γ grows significantly larger as the chemical potential gradually shifts away from the surface Dirac point. After a NO_2 exposure of 0.15 Langmuir (0.15L) (Fig. 5 (f)), the chemical potential is raised by approximately 170 meV. The surface conduction bands gain partial occupation, introducing a weak resonant state feature near

E_F . The pure surface band velocity is unchanged after NO_2 exposure. However, the surface Dirac point (degenerate Kramers' point) is rigidly shifted downwards to 300 meV below E_F . Increasing amounts of NO_2 doping increase the electron carrier density on the Bi_2Te_3 surface. Eventually, after an exposure of 1 L of NO_2 (Fig. 5 (i)), the surface Dirac point reaches 350 meV below E_F . Inside the non-degenerate Dirac cone, a pair of spin-split parabolic bands from the previously unoccupied surface conduction band is also observed at around 60 meV. Additional exposures deteriorates the sample significantly. While the position of the Dirac point becomes difficult to locate, judging from the size of the lowest energy electron pocket the shift of the Fermi level is minimal with further dosages. This observation is in direct contrast with that observed in graphene [21], where electrons are transferred from the graphene layer to the NO_2 molecules.

We then estimate the amount of charge carrier transfer as a result of NO_2 deposition by applying the Luttinger count theorem. Relaxing the sample for 1 hour after cleavage, the charge concentration (figure 5 (e)) is approximately 0.00335 electrons per unit cell. After exposure to 1 L of NO_2 gas (Fig. 5 (i)), the surface becomes strongly electron doped and approximately 0.039 electrons are transferred to the surface. The mechanism behind this charge transfer is presently unclear which makes it difficult to precisely estimate the amount of NO_2 molecules that actually dopes the surface. Nevertheless, it is clear that a systematic tuning of the chemical potential is possible with K doping.

We have further investigated the effect of photo-induced changes on the surface of Bi_2Te_3 . In our experiment, we find that the effect of NO_2 adsorption is unstable against photon exposure. This result suggests that photo-induced doping could be an additional way with which to tune the electron-doped surface states on Bi_2Te_3 (111). We present the photon-induced evolution of the surface band structure data in Fig. 6. To reduce the uncertainties due to photon-related effects, each spectrum was collected within 1 minute after opening the photon shutter. Fig. 6 (a) presents the surface band dispersion after the sample was first exposed to 0.3 L of NO_2 . The resulting Dirac point is at about 330 meV below E_F . With photon exposure the chemical potential gradually shifts upwards. After a dosage of 1×10^{15} photons 30 eV , the Dirac point is shifted to approximately 250 meV below E_F . Successive exposures continue to shift the chemical potential. After a total dosage of approximately 8×10^{15} photons per mm^2 , the chemical potential is found to be stabilized as the Dirac point reaches 130 meV, the energy location prior to the NO_2 exposure. The photon-induced

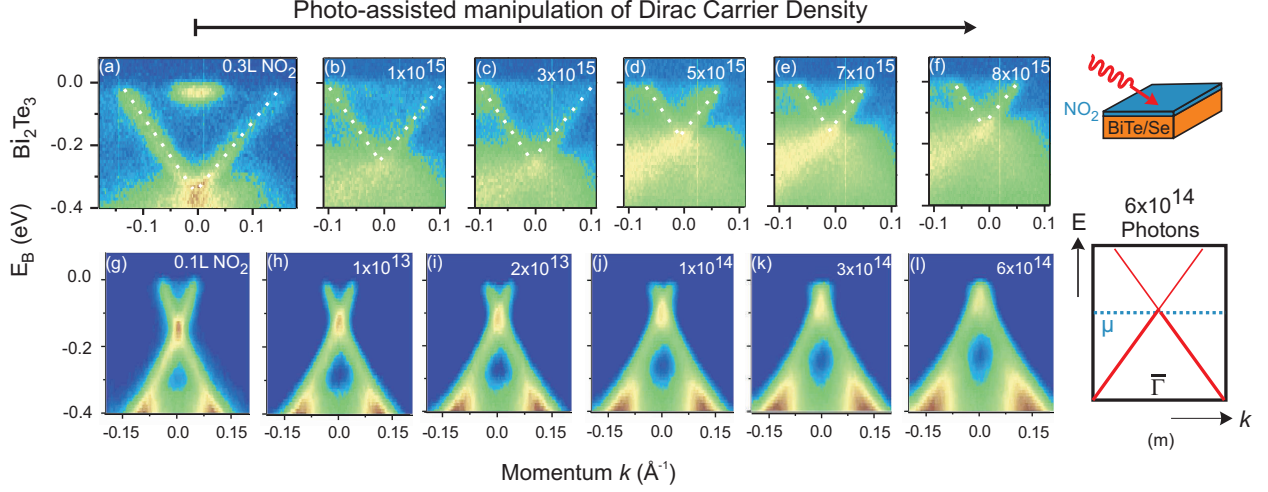


FIG. 3: Photo-induced manipulation of the topological surface states on Bi_2Te_3 : (a) Upon exposures of 0.3L of NO_2 on Bi_2Te_3 , the Dirac point is located at approximately 330meV below E_F . (b)–(f) Photon exposure reverses the electron transfer to the Bi_2Te_3 surface, moving the surface chemical potential in a well-controlled manner shifting towards the Dirac point. With a dosage total of (b) 1×10^{15} photons, the Dirac point is moved to 250meV below E_F . The Dirac point eventually reaches the energy-location prior to the NO_2 exposure with a dosage of 8×10^{15} photons, which is at about 130meV below E_F . For comparison, the photo-induced doping of Bi_2Se_3 surface states exposed with (g) 0.1L of NO_2 gas is also presented in (h)–(l). With a dosage level of (i) 2×10^{13} photons, the Dirac point is shifted by 50meV to 100meV below E_F . The chemical potential is eventually stabilized at the Dirac point by the application of 6×10^{14} photons per m^2 .

effective doping is observed for a wide range of UV energies (28–55 eV) and is found to be robustly reproducible.

For comparison with other topological insulators that may have a different chemically-active surface with different relaxation details, we present the effect of photo-induced doping on the Bi_2Se_3 (111) surface doped with NO_2 molecules (Fig. 6 (g)–(l)). Previous systematic study [22] has shown that exposure to NO_2 dopants hole-dopes the Bi_2Se_3 surface states, moving the chemical potential to the Dirac point. While this behavior is opposite to that observed for our Bi_2Te_3 (telluride system), the additional effect of photodoping is similar for both systems. In Figure 6 (g) we present the surface band dispersion data taken after a fixed dosage of 0.1L of NO_2 . The resulting Dirac point is at a binding energy of approximately 150meV. Similar to Bi_2Te_3 , photo-induced doping gradually moves the chemical potential

downwards. A dosage of 2×10^{13} photons at 30eV shifts the Dirac point by 50meV, while a total dosage of 6×10^{14} photons shifts the Dirac point to the Fermi level (Fig. 6(l)). While the effect of photo-induced doping in Bi_2Te_3 could be attributed to photo-stimulated desorption, the detailed mechanism in Bi_2Se_3 is still under investigation by us. Nevertheless, we have demonstrated that photon-induced hole doping can be a controllable mechanism to manipulate the topological spin-polarized surface bands, systematically driving the chemical potential to the Dirac point via photon flux.

In summary, using high resolution ARPES, we have demonstrated for the first time a suite of methods to controllably manipulate the topological edge states of the topological insulator Bi_2Te_3 on its (111)-surface without breaking time reversal symmetry. Our systematic data (Fig.1-3) directly show that both potassium (K) and NO_2 electron-dopes the topologically ordered surface over a wide doping-range. Additionally, we showed that the effect of the dosage can be reversed by controlling exposure to photon flux. We further showed that photodoping has a similar effect on Bi_2Se_3 , which can be used to place the chemical potential to the much desired Dirac point. Our work opens up many new possibilities for future utility of topological insulators in spintronic and quantum computing research. More importantly, our methods of topological surface state manipulation are highly suitable for spectroscopic studies than the traditional electrical gating based techniques thus open up new spectroscopic investigation opportunities of topological quantum phenomena.

NOTE ADDED : Some of the methods and their combinations demonstrated here can be successfully applied to other topological insulators such as the bulk-insulating Bi_xSb_x , Sb_2Te_3 and Bi_2Se_3 by carefully considering their unique material-specific surface chemistry and the nature of the surface relaxation which will be shown elsewhere [22].

-
- [1] J.E.Moore, "Topological Insulators: The Next Generation" Nature Phys. 5, 378 (2009).
 - [2] S.-C. Zhang, "Topological States of Quantum Matter" Physics 1, 6 (2008).
 - [3] C.L.Kane, "An insulator with a twist" Nature Phys. 4, 348 (2008).
 - [4] L.Fu, C.L.Kane and E.J.Mele, Phys. Rev. Lett. 98, 106803 (2007).
 - [5] J.E.Moore and L.Balents, Phys. Rev. B 75, 121306(R) (2007).
 - [6] L.Fu and C.L.Kane, Phys. Rev. B 76, 045302 (2007).

- [7] X.-L. Qi, T. L. Hughes and S.-C. Zhang, *Phys. Rev. B* 78, 195424 (2008).
- [8] L. Fu and C. L. Kane, *Phys. Rev. Lett.* 102, 216403 (2008).
- [9] B. Seradjeh, J. E. Moore and M. Franz, *arXiv:0902.1147* (2009).
- [10] D. Hsieh, D. Qian, L. Wray, et al.; *Nature* 452, 970 (2008).
- [11] Y. Xia, D. Qian, D. Hsieh, et al.; *Nature Phys.* 5, 398 (2009).
- [12] D. Hsieh, Y. Xia, L. Wray et al.; *Science* 323, 919 (2009).
- [13] H.-J. Noh, H. Koh, S. J. Oh et al.; *Europhys. Lett.* 81, 57006 (2008).
- [14] D. Hsieh, Y. Xia, D. Qian, et al., *arXiv:0904.1260* (2009).
- [15] Y. L. Chen, J. G. Analytis, J. H. Chu et al., *arXiv:0904.1829* (2009).
- [16] B. A. Bernevig, T. L. Hughes, S. C. Zhang, *Science* 314, 1757 (2006);
- [17] P. Blaha et al., computer code WIEN2K (Vienna University of Technology, Vienna, (2001).
- [18] H. Zhang, C.-X. Liu, X.-L. Qi, X. Dai et al., *Nature Phys.* 5, 438 (2009).
- [19] J. P. Perdew, K. Burke and M. Ernzerhof, *Phys. Rev. Lett.* 77, 3865 (1996).
- [20] T. Ohta, A. Bostwick, T. Seyller et al.; *Science* 313, 951 (2006).
- [21] S. Y. Zhou et al.; *Phys. Rev. Lett.* 101, 086402 (2008).
- [22] D. Qian, D. Hsieh, Y. Xia et al., (surface doping measurements, 2008). Some preliminary surface-doping data and methods were presented at the KITP conferences : (<http://online.itp.ucsb.edu/online/lowdim09/hasan/>) and (<http://online.itp.ucsb.edu/online/qspinhallm08/hasan/>) (2008).

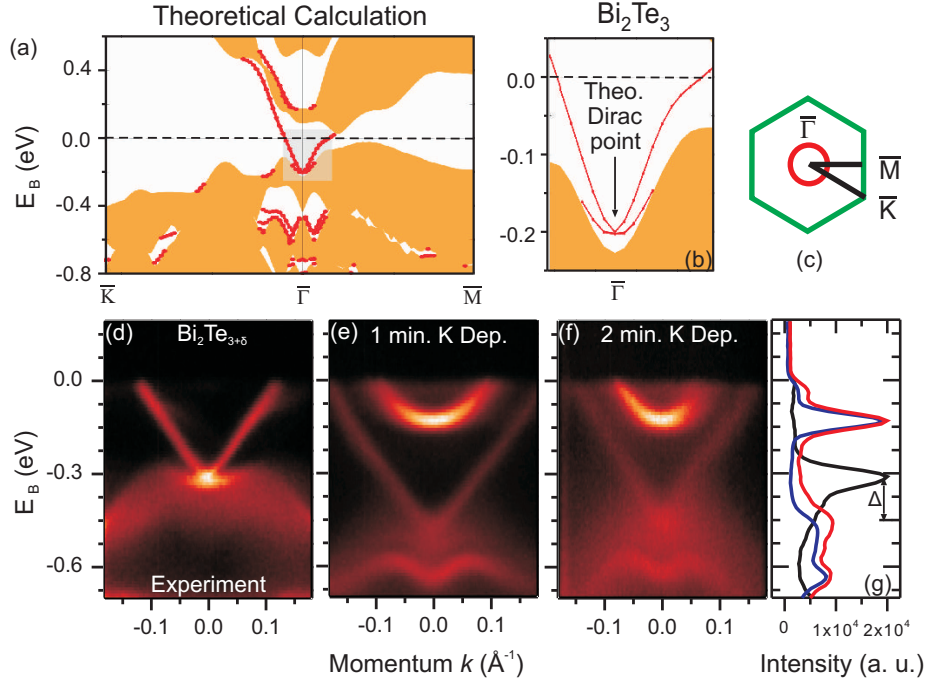


FIG . 4: (Enlarged version of Fig-1) Electron doping via potassium (K) deposition on Bi₂Te₃ [111] topological surface : (a)–(b) (111) Surface band (red lines) calculation with spin-orbit coupling shows a pair of non-degenerate Dirac bands crossing the E_F . The bulk band projection is denoted by the shaded region in orange. The resulting (c) Fermi surface is a single non-degenerate ring centered at the zone center. (d) ARPES data on Bi₂Te_{3+δ} shows a slight rise of the chemical potential relative to the stoichiometric compound Bi₂Te₃ [14]. The surface band structure after depositing potassium (K) for (e) one minute and (f) two minutes show additional electron-doping of the surface states. The (g) energy distribution curves at show that relative to the pristine sample (black), the chemical potential is shifted by 140 meV after one minute of (red) K deposition. Only a small additional shift of the E_F position is observed upon an additional minute of K deposition (blue).

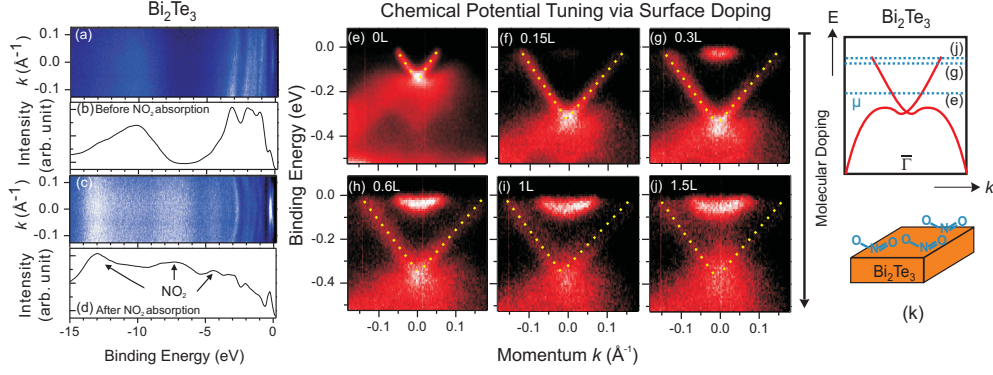


FIG. 5: (Enlarged version of Fig-2) Manipulation of Bi_2Te_3 [111] topological surface via molecular adsorption: (a) Angle-resolved valence band spectra (a) prior to and (c) post exposure to 1.5 Langmuirs of NO_2 . Panels (b) and (d) show the angle integrated spectra for (a) and (c), respectively. Prior to the NO_2 adsorption, the valence band features are sharp and dispersive with momentum. After exposure to NO_2 gas, three non-dispersive features appear at binding energies of 4.4 eV, 7.5 eV and 13 eV. High resolution surface band dispersion data near the Γ point suggest (e) two non-degenerate surface bands intersecting at 130 meV below E_F , forming a Dirac point. (f)–(j), with NO_2 adsorption, the chemical potential is systematically raised, thereby introducing additional electrons into the Bi_2Te_3 surface bands. The Dirac point moves away from E_F with increasing amounts of NO_2 exposure. At 1 Langmuir dosage value, the lowest surface conduction band gains electron occupation, and the Dirac point reaches 350 meV below E_F .

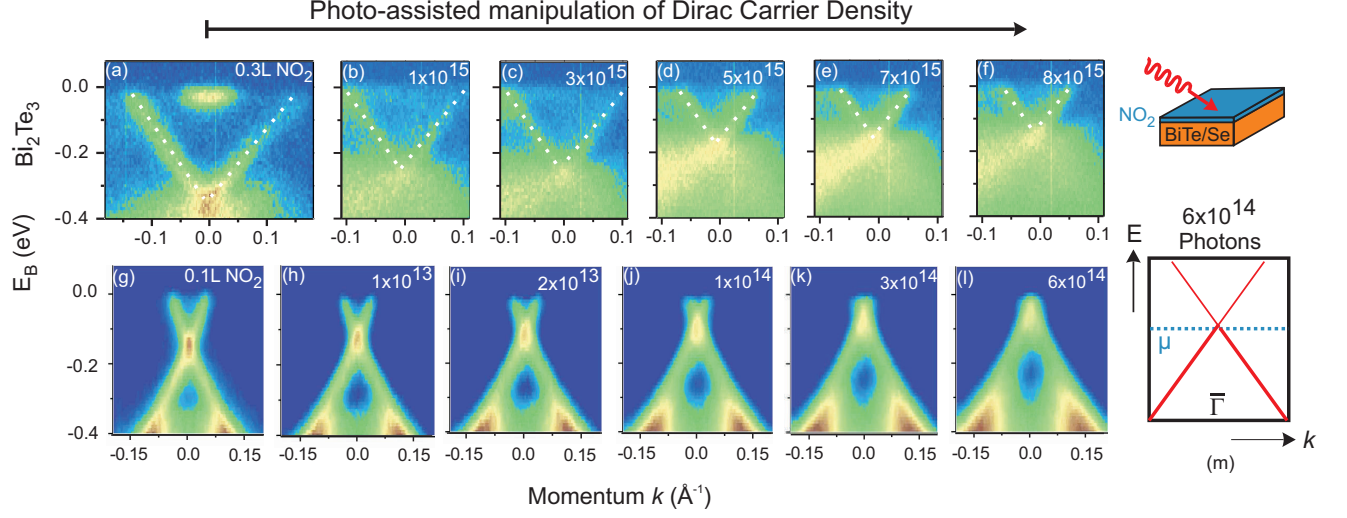


FIG . 6: (Enlarged version of Fig-3) Photo-induced manipulation of the topological surface states on Bi_2Te_3 : (a) Upon exposures of 0.3L of NO_2 on Bi_2Te_3 , the Dirac point is located at approximately 330meV below E_F . (b)–(f) Photon exposure reverses the electron transfer to the Bi_2Te_3 surface, moving the surface chemical potential in a well-controlled manner shifting towards the Dirac point. With a dosage total of (b) 1×10^{15} photons, the Dirac point is moved to 250meV below E_F . The Dirac point eventually reaches the energy-location prior to the NO_2 exposure with a dosage of 8×10^{15} photons, which is at about 130meV below E_F . For comparison, the photo-induced doping of Bi_2Se_3 surface states exposed with (g) 0.1L of NO_2 gas is also presented in (h)–(l). With a dosage level of (i) 2×10^{13} photons, the Dirac point is shifted by 50meV to 100meV below E_F . The chemical potential is eventually stabilized at the Dirac point by the application of 6×10^{14} photons per mm^2 .